

# Performance of Cassini Reaction Wheel Friction Compensation Scheme during Spin Rate Zero-crossing and Drag Spikes\*

Allan Y. Lee<sup>1</sup>

*Jet Propulsion Laboratory, California Institute of Technology, Pasadena, CA 91109-8099*

Cassini uses reaction wheels to achieve the spacecraft pointing stability that is needed during imaging operations of several science instruments. The Cassini flight software makes inflight estimates of reaction wheel bearing drag torque and the reaction wheel controller uses these estimates to achieve a high level of spacecraft pointing stability. However, the Cassini drag torque estimator was designed to accurately track the bearing drag torque only in the steady state. When the physical drag torque changes abruptly (for example, during a reaction wheel spin rate reversal or when wheel bearings experienced drag spikes), the drag estimator will not be able to track the physical drag closely. This will lead to a degradation in the spacecraft pointing stability performance. For Cassini, this was not a problem because of the significant performance margin in pointing stability. However, for missions that have very challenging pointing stability requirements and that must perform well in the presence of frequent wheel rate reversals, alternative drag-compensating control schemes must be considered. To this end, alternative drag torque compensating control schemes (such as the adaptive model reference control scheme) are briefly reviewed in this paper. Selected design features used in these friction compensation schemes may be incorporated in reaction wheel controller design to improve the robustness of spacecraft pointing stability performance with regard to a wide range of reaction wheel drag torque anomalous behavior.

Keywords: Adaptive system, Attitude control system, Cassini, Command-shaping, Dahl friction, Dither, Drag spikes, Friction compensation, Pointing stability, Reaction wheel, Stiction friction, Zero-crossing.

## I. Introduction

As the first spacecraft to achieve orbit at Saturn in 2004, Cassini has collected science data throughout its four-year prime mission (2004–08), and has been approved for two extended missions.<sup>1</sup> The first extended mission called the Cassini Equinox Mission was completed in September 2010. The second extended mission called the Cassini Solstice Mission was completed in September 2017. On September 15, 2017, Cassini dived into the Saturn's atmosphere, sending back science data for as long as its thrusters can keep the spacecraft's antenna pointed at Earth, and burnt up and disintegrated like a meteor.

Cassini uses reaction wheels to achieve the spacecraft pointing stability that is needed during imaging operations of several science instruments. The Cassini flight software makes in-flight estimates of reaction wheel bearing drag torque and made them available to the reaction wheel controller to achieve a high level of pointing stability.<sup>2</sup> Since its launch on October 15, 1997, the performance of the Cassini AACS design has been superb. All pointing stability requirements of the narrow angle camera are met with significant margin.<sup>3</sup>

---

\*Copyright 2017 California Institute of Technology. Government sponsorship acknowledgement.

<sup>1</sup>Section Staff, Guidance and Control Section, Division of Autonomous Systems. Mail Stop 230-104, 4800 Oak Grove Drive, Pasadena, CA 91109-8099, USA. Project Element Manager, Cassini Attitude and Articulation Control Mission Operations Team, 1999–2009. Allan.Y.Lee@jpl.nasa.gov.

However, the Cassini drag torque estimator was designed to accurately track the bearing drag torque *only in the steady state*. When the physical drag torque changes abruptly due to, for example, a spin rate reversal (“zero-crossing”), the drag estimator can still track the physical drag torque but there will be significant transient tracking error of the drag torque. The faster the drag torque changes, the larger will be the tracking error.<sup>4,6</sup> As a result, the drag torque estimator will not be able to fully compensate the physical drag, and the spacecraft pointing stability performance will suffer as a result. For Cassini, this was not a problem because of the large performance margin mentioned above. However, for missions with very challenging pointing stability requirements and must perform well in the presence of abrupt drag torque changes, alternative drag-compensating control schemes must be considered. An important class of scenarios to consider is when the spacecraft performs a flyby of a planetary moon. Typically, a camera or the high-gain antenna mounted on the spacecraft will be nadir-pointed at a target throughout the motion. Hence, the nadir axis will require a slew angle of  $180^\circ$  in an inertial frame. In these flyby scenarios, as illustrated in Appendix A, there will be zero-crossing of the reaction wheel’s spin rate. The resultant attitude perturbations will degrade the S/C pointing stability performance just at the time when camera must perform critical imaging of the target.

Since the year 2000, all Cassini RWA bearings experienced a class of anomalous drag torque that were generally “spiky” in nature.<sup>4</sup> The initial sudden rise in drag torque was often followed by either a rapid (several minutes) or gradual (several hours) exponential decay to the nominal drag level. In these scenarios, again, the implemented Cassini RWA drag torque estimator could not fully compensate for these drag spikes, and the spacecraft attitude control and stability performance degraded. Many other spacecraft had experienced anomalous reaction wheel bearing drag torque symptom similar to those of Cassini (e.g., XMM-Newton, Rosetta, DAWN, and others mentioned in Ref. 4). For example, beginning in April 2013, the Solar Dynamics Observatory (SDO) operations and instrument teams began observing an increase in spacecraft jitter that was ultimately traced back to anomalous behavior in one of its reaction wheels believed to be related to fluctuations in bearing friction.<sup>5</sup> Since it is hard to completely avoid having bearing drag spikes during operations, it is important to have a drag torque estimator that can track transient drag “spikes” as well as possible.

In this paper, sets of anomalous Cassini wheel bearing drag torque signatures that had been observed in flight will first be described.<sup>4</sup> Then, telemetry that shows the impacts these bearing drag torque had on the spacecraft attitude and attitude rate will be presented. Finally, a limited-scope literature survey of friction-compensating control strategies that had been found in past research works that can maintain the low-velocity tracking performance of a pointing system in is given. To this end, six different friction-compensating control schemes are briefly reviewed in this paper. They are: [1] Use of a high-gain velocity control loop, [2] estimation-based friction compensation system, [3] adaptive friction compensation system, [4] extended Kalman-Bucy filter-based compensation system, [5] use of a shaped drag torque compensation command, and [6] the use of a dither signal. Not surprisingly, past research had indicated that all these control schemes can outperform traditional linear control systems. Selected design features used in these control schemes may be incorporated in a reaction wheel controller design to improve the robustness of spacecraft pointing stability performance relative to a wide range of reaction wheel drag torque nonlinear behavior.

## II. Cassini Reaction Wheel Controller Design<sup>2</sup>

The reaction wheel assemblies are used primarily for attitude control when precise and stable pointing of a science instrument is required during the prime mission phase. Because the spacecraft’s principle axes are very closely aligned with the spacecraft’s mechanical axes, the basic structure of the Reaction Wheel Attitude Control System (RWAC) is a decoupled, three-axis, Proportional and Derivative (PD) controller. Fig. 1 is an illustration of the RWAC design.<sup>2</sup> Due to the presence of bearing drag torque in the reaction wheels, a controller with the “PD” control architecture will not be able to drive the spacecraft attitude control error to zero unless an integral term is added to the PD controller. This difficulty was overcome by the addition of a Proportional and Integral (PI) estimator of the bearing drag torque in the flight software. In effect, integral control action is added “locally” to remove any steady-state spacecraft attitude control errors. Fig. 2 is a simplified illustration of the drag torque estimator design.<sup>6</sup> As illustrated in Fig. 2, the estimated bearing drag torque is added to the S/C’s attitude control torque ( $T_{\text{Control}}$ ) to form the total torque command ( $T_{\text{Total}}$ ). The total torque is sent to the RWA D.C. motor. With this control architecture, if the bearing drag torque is elevated due to anomalous bearing performance, a larger motor torque command will be sent. As a result, impacts of the anomalous bearing drag on the S/C attitude control performance is

minimized. The estimated drag torque is also made available via telemetry to the mission operations team. Ground operators trend this and other RWA data (e.g., bearing temperatures) to monitor the long-term health of the reaction wheels. The RWAC design has a bandwidth of 0.0299 Hz (in Fig. 1,  $K_p = 0.2273$  rad/s and  $K_d = 0.1557$  rad/s). The gain and phase margins of RWAC are 10 dB and  $30^\circ$ , respectively.<sup>2</sup>

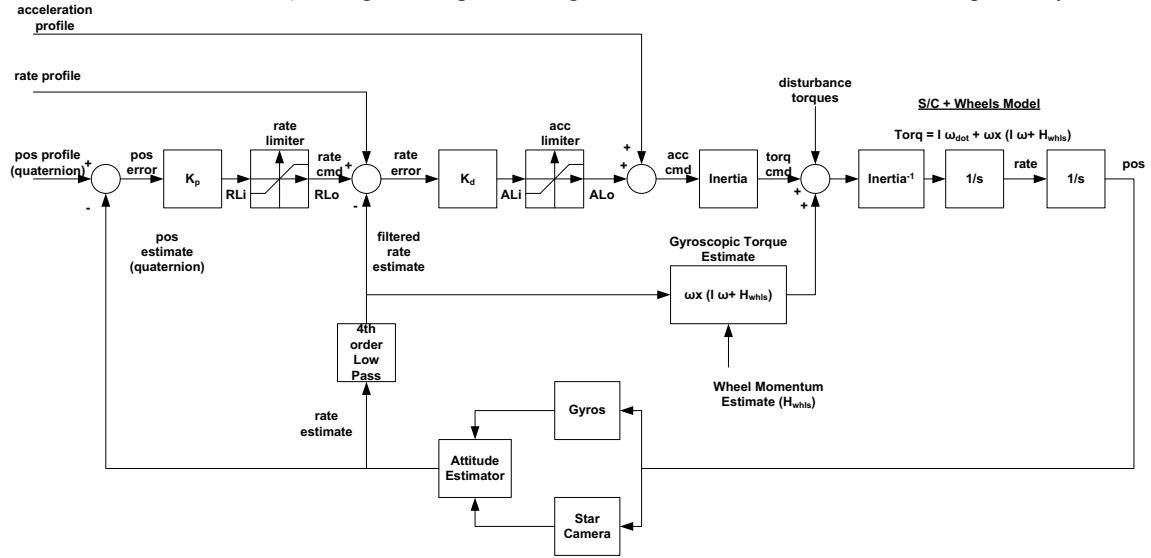


Fig. 1. Block Diagram of the Reaction Wheel-based Attitude Control System<sup>2</sup>

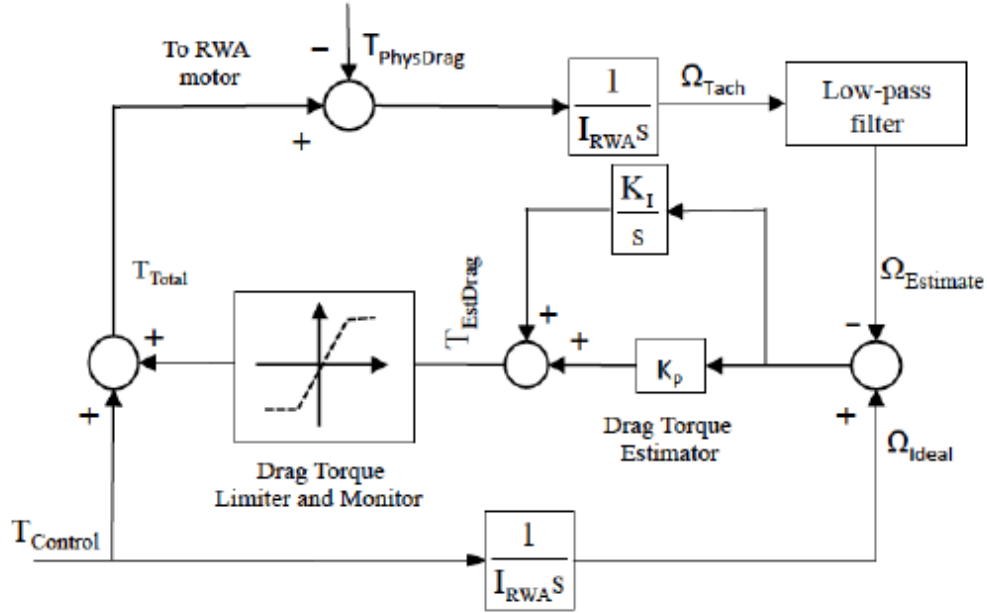
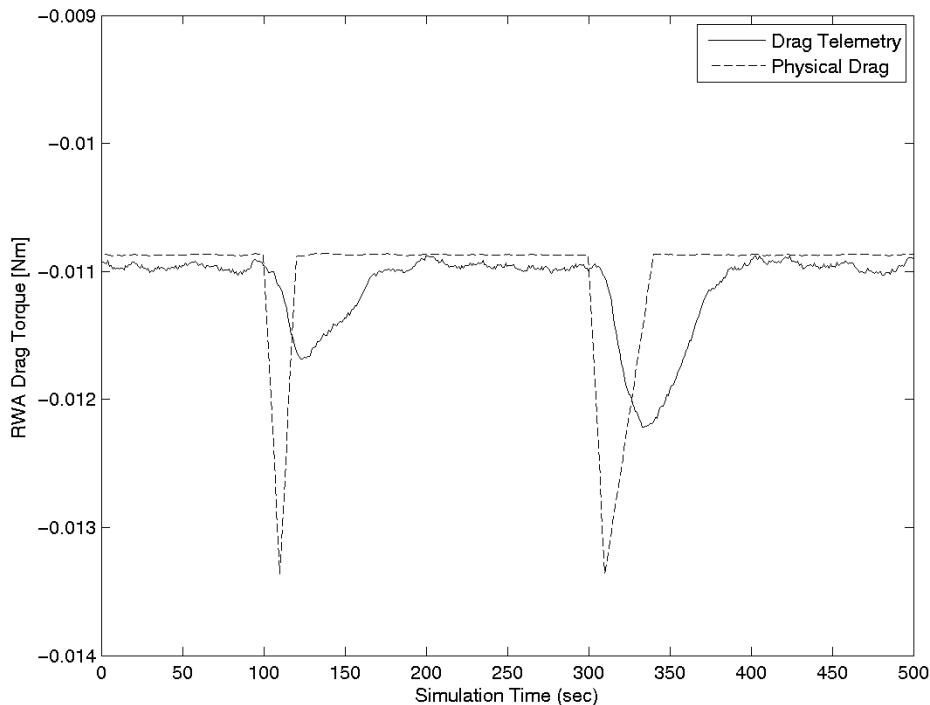


Fig. 2. Block Diagram of the Reaction Wheel Hardware Manager Design<sup>6</sup>

The drag torque estimator was designed to accurately track the physical bearing drag torque only in the steady state. When the physical drag torque changed due to varying RWA spin rate (or experienced anomalous drag “spikes”), the drag estimator can still track the physical drag torque but there will be a tracking error. Let  $T_{Phy}(s)$  and  $T_{Est}(s)$  be the Laplace transforms of the physical and estimated drag torques, respectively. From Fig. 2, we have:<sup>4,6</sup>

$$\frac{T_{Est}(s)}{T_{Phy}(s)} = \frac{K_p s + K_I}{I_{RWA} s^2 + K_p s + K_I} = \frac{2\xi_D \omega_D s + \omega_D^2}{s^2 + 2\xi_D \omega_D s + \omega_D^2} \quad (1)$$

In this expression,  $K_p$  and  $K_i$  are the gains of the PI drag torque estimator, and  $I_{RWA}$  is the moment of inertia of each reaction wheel's rotor. The gains are selected to be:  $K_p = 2\xi_D\omega_D I_{RWA}$  and  $K_i = \omega_D^2 I_{RWA}$ . Here,  $\omega_D$  and  $\xi_D$  are the bandwidth and damping ratio of the drag torque estimator design ( $\omega_D = 0.01$  Hz and  $\xi_D = 0.707$ ). As an example, Fig. 3 depicts the time history of the estimated drag torques  $T_{Est}(t)$  in response to two similar but different "triangular impulse" drag torques  $T_{Phy}(t)$ . Both impulses rise from the nominal drag level to a peak drag level with a "delta" of -2.5 mNm in 10 s. Thereafter, the first and second drag impulses fall linearly from their respective peaks back to the nominal level in 10 and 30 s, respectively. As depicted in Fig. 3, the first estimated peak drag "delta" is about 0.6 mNm which is only 24% of the actual drag torque "delta." The second estimated peak drag "delta" is about 1.2 mNm which is 48% of the actual peak torque "delta." Their "settling" times are 70–80 s, significantly longer than the actual time.



**Fig. 3. Time Histories of Estimated RWA Drag Torques<sup>4</sup>**

### III. Cassini Attitude Control Performance during RWA Spin Rate Zero Crossing

In Fig. 4, there was a "zero crossing" of the RWA-4 rate at 2013-DOY-005T18:24:11 (as indicated by a bold arrow head), from the clockwise (CW) to the counter-clockwise (CCW) direction.<sup>6</sup> The crossing happened at a rate of +1.73 rpm per second.<sup>#</sup> As a result of the incomplete RWA-4 drag torque compensation, noticeable perturbations in all three per-axis S/C's attitude control errors were observed immediately after the crossing. About the X-axis, there was a S/C attitude perturbation of -11  $\mu$ rad in 9.5 s. Hence, the X-axis rate perturbation is -1.16  $\mu$ rad/s. Those about the Y and Z-axis are +0.87 and -1.48  $\mu$ rad/s, respectively. The MOI's of the S/C about the X, Y, and Z-axis are (in the year 2013) [6,400, 5,300, 3,500] kg-m<sup>2</sup>, respectively. The angles between the spin axis of RWA-4 and the S/C's X, Y, and Z-axis are [45°, 114.1°, 54.74°], respectively. Using the estimated rate perturbations about the S/C's X, Y, and Z-axis, the estimated torque impulses due to the zero-crossing are -10.5, -11.3, and -8.95 milli-Nms, respectively. The mean value of the torque impulse is -10.3 milli-Nms.

<sup>#</sup>Experiment results reported in Ref. 28 indicate that the zero-crossing torque impulse is related to the crossing rate. Hence, the crossing rate is recorded here.

The perturbations in the S/C's attitude control errors observed during RWA-4 spin rate zero-crossing may be explained as follows: At the time when the RWA-4 rate slowed from a small CW spin rate (say, 1-2 rpm) toward and reached zero rpm, the control torque was at a level needed to overcome stiction drag torque in the CW direction. When the wheel stopped, the spacecraft attitude about the RWA-4 axis is no longer being controlled. As a result, all three per-axis attitude control errors began to diverge (see Fig. 4). The star tracker detected this growing attitude error and will command the D.C. motor of RWA-4 to issue more control torque. The "extra" torque is needed to compensate for the incomplete drag torque compensation due to the abrupt nature of zero-crossing drag. The process took some time because there must be enough accumulated attitude errors to generate control torque to first reduce the initial control torque (that was needed to overcome the CW stiction drag) to zero, and then to increase the motor torque to a level needed to overcome the CCW drag torque in the opposite direction. During this process, the RWA-4 was stopped momentarily (but it will be very hard to spot that in the RWA-4 spin rate telemetry due to the "noisiness" of the data). Once the CCW stiction drag is overcome by the RWA-4 motor, the reaction wheel will begin to move and get away from the "zero crossing" condition.<sup>#</sup> At that time, full spacecraft attitude control was regained and all per-axis attitude control errors began to fall to a nominal level.

The instrument CIRS (Composite Infrared Spectrometer) has a stability requirement of 100  $\mu$ rad over 22 s ( $2\sigma$  per axis).<sup>1,3</sup> This corresponds to a rate change requirement of not more than  $\approx 4.6 \mu$ rad/s. The boresight axis of CIRS is aligned with the S/C's -Y-axis.<sup>1</sup> Hence, the instantaneous velocities of the S/C about the X and Z-axis must not exceed 4.6  $\mu$ rad/s. From the back-of-envelop calculations made above, the velocity changes due to the zero crossing had magnitudes of 1.16-1.48  $\mu$ rad/s about these two axes. Hence, for CIRS (and other remote-sensing science instruments), the observed crossing-related perturbed rates were not be a problem. However, for missions without the benefit of large performance margin, a more capable drag torque estimator that can better track transient drag "spikes" will be needed.

Two additional examples of perturbations in Cassini's attitude control errors observed during RWA spin rate zero-crossing are given in Appendix B.

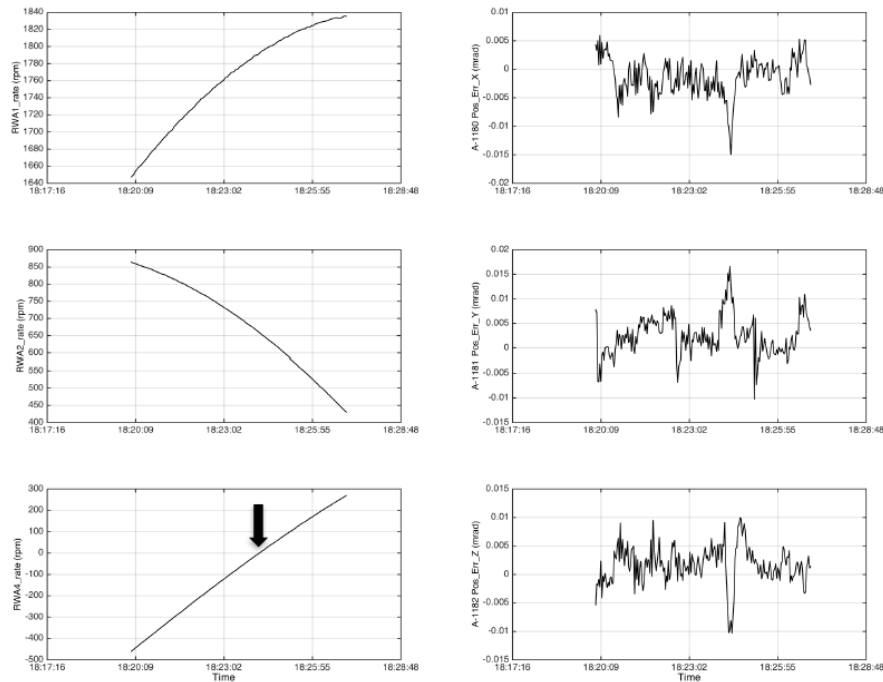


**Fig. 4. Transients of S/C Attitude Errors Caused by RWA-4 Rate Reversal on 2013-DOY-005.<sup>6</sup>**

<sup>#</sup>The extra X-axis control torque needed could be estimated by  $K_p K_d I_{xx} \dot{\theta}_x$  or  $0.2273 \times 0.1557 \times 6,400 \times 1 \text{e-}6 \approx 2.49 \text{ mNm}$ . The values of  $K_p$  and  $K_d$  cited were given in Section II. The peak X-axis attitude control error depicted in Fig. 4 was 11  $\mu$ rad. About the RWA-4 axis, the "extra" D.C. motor torque is  $2.49/\cos 45^\circ = 3.52 \text{ mNm}$ .

Cassini is not alone. Operations teams of other missions had made similar observations. On February 16, 2014, RWA-4 of the SDO spacecraft also had a zero-crossing.<sup>5</sup> The crossing was accompanied by spikes in the spacecraft attitude error of  $\approx -58 \mu\text{rad}$  ( $-12 \text{ } \mathcal{S}\mathcal{E}\mathcal{C}$ ) about the roll axis and  $-34 \mu\text{rad}$  ( $-7 \text{ } \mathcal{S}\mathcal{E}\mathcal{C}$ ) about the pitch axis (see Fig. 5). The perturbation was large enough to briefly trip the onboard fault detection system. Further investigation showed that upon RWA-4 reaching zero rpm, the ACS controller began issuing RWA4 progressively larger torque commands with no response from the wheel until the commanded torque reached a value of  $\approx 26$  milli-Nm. At this point the wheel suddenly began rotating again, and the aforementioned attitude disturbance was induced on the spacecraft.

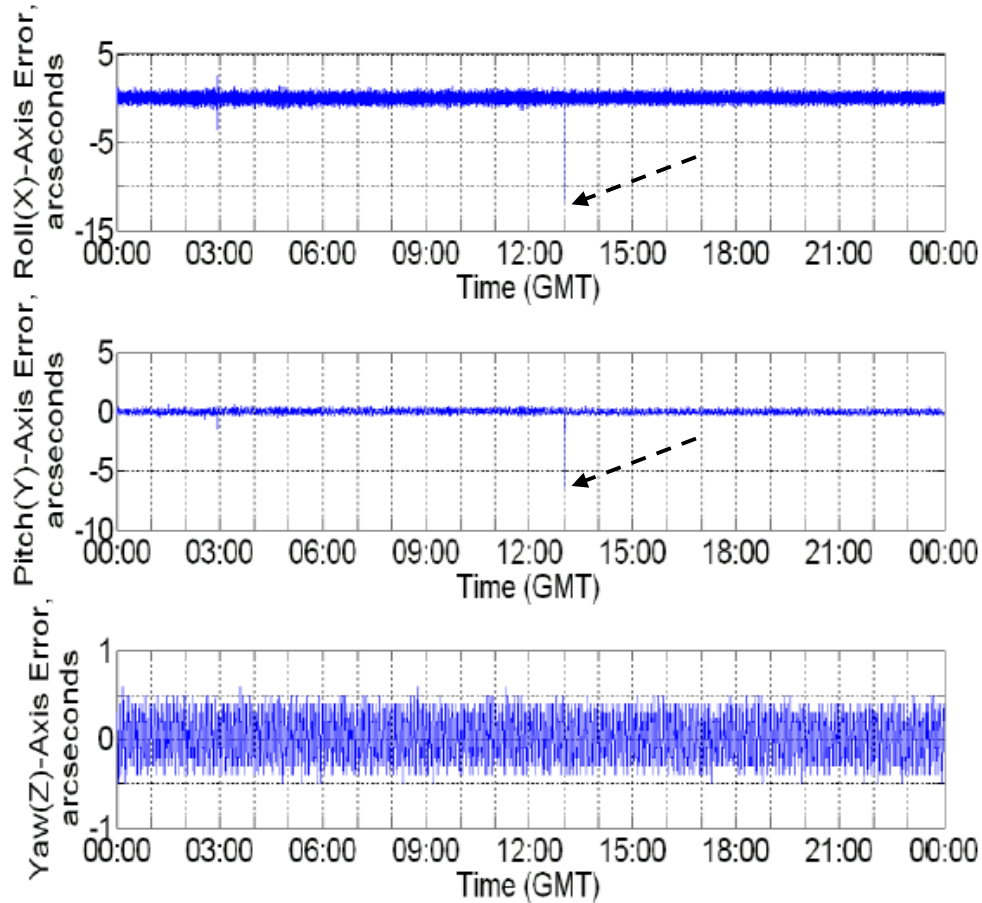


**Fig. 5. SDO Attitude Transients Caused by A RWA Rate Reversal (Note the large attitude control error transient at 13:00 GMT)<sup>5</sup>**

#### IV. Cassini Reaction Wheel Drag Torque Spikes

There is a class of anomalous drag torque signatures that appeared in the RWA drag telemetry since the year 2000. This class of anomalous drag torques is “spiky” in appearance, and the drag spikes usually occurred at time when the wheels were maintained at a constant spin rate. In a constant-spin rate condition, the expected drag torque should be nearly constant. This is indeed the case, but at times drag torque spikes were observed superimposed on the “constant” drag torque. Typically, the drag “spike” consists of an initial impulsive rise in drag magnitude followed by either a rapid (several minutes) or gradual (several hours) decay in magnitude to its nominal drag torque level. Sometime later, another drag spike, possibly with a different magnitude, will appear, and a drag torque “train” is formed. The spikes had a wide range of magnitudes and they occurred in a wide range of RWA spin rate conditions. Two sub-classes of anomalous drag torque spikes are described below.

Depicted in the top subplots of Fig. 6 are the time histories of the RWA-4 spin rate and drag torque observed on 2004-DOY-041 when the wheel was maintained at an almost-constant rate of +271 rpm. Without any clear cause, several drag spike transients (as indicated by a bold arrow head) with magnitudes of 0.2–1.5 mNm were observed. These spikes decayed to the nominal level quickly, in 6.5–7 min. The second class of anomalous drag spikes was also “spiky” in nature but they had significantly longer “settling” times. Depicted in the bottom subplots of Fig. 6 are the time histories of RWA-1 spin rate and drag torque observed on 2006-DOY-266 when RWA-1 was maintained at an almost-constant rate of -250 rpm when a set of anomalous drag spikes (as depicted by a bold arrow head) were observed. The magnitudes of these spikes were about 6–7 mNm. These drag spikes decayed to the nominal level slowly, in about 1.4–1.5 hour (instead of several minutes).

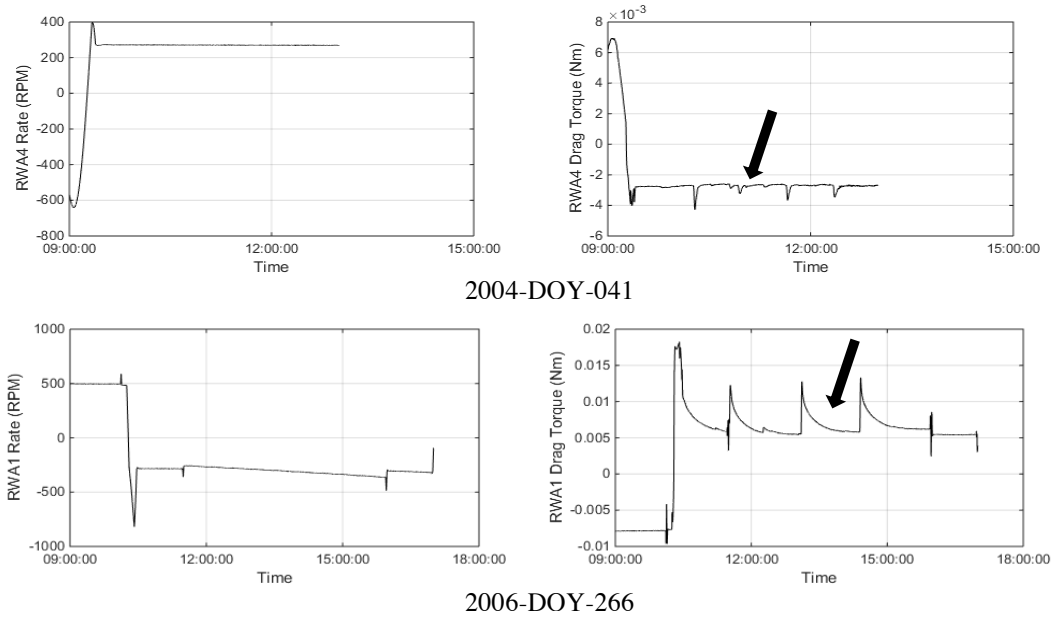


**Fig. 6. Spiky RWA-4 and RWA-1 Drag Torque Observed<sup>4</sup>**

The most pronounced characteristic of the drag spikes is that they have an abrupt onset followed by an exponential decay. The definite cause of these drag torque spikes is unknown. Our conjecture is that it is an “oil jog” phenomenon: a rapid incorporation of some quantity of lubricant by the bearings followed by its relatively slow dispersal. Bearings can have small pockets of lubricant that collect outside of the normal ball/cage and ball/race contact areas. They can become entrained in the contact areas by a variety of processes. Bearings that suddenly encounter an addition of oil will show an abrupt increase in drag that will then dissipate. The size of the drag torque spike and the time required to redistribute the oil depend on the amount of oil in question and the RWA spin rate at the time the spike occurred. If this conjecture is right, it is actually a positive indication of the presence of useful oil in bearings.<sup>4</sup> However, if the drag spike is large, it might be an indication that some of the lubricant is congealed. Cassini mission operation team has trended the magnitudes and occurrence frequency of these drag spike events. The spikes observed have a wide range of magnitude, and they occurred in a wide range of RWA spin rates. The incidence of these drag spike events did not decline over time as the bearings accumulate run time. Hence, it is important to have in the RWAC a friction-compensating scheme to mitigate the impacts of these spikes on the S/C’s pointing stability.

#### **IV.1 Incomplete Compensation of a Large Drag Spike Could Trigger Fault Protection**

On 2004-DOY-212 (July 31, 2004), Cassini was commanded to perform a continuous Z-axis roll using RWA-1, 2, and 4. Science observations during this rolling motion do not require meeting any tight S/C pointing stability requirement. Hence, small perturbations in the S/C attitude errors due to incomplete compensation of the drag torque spikes are not very important in this scenario. However, incomplete compensation of drag torque spikes can create another kind of S/C problem: triggering a fault protection

error monitor. During this rolling motion, RWA-1 rate fluctuated between -764 and -1194 rpm, which are well outside the sub-EHD region ( $\pm 300$  rpm). Nevertheless, the estimated RWA-1 drag was found to be significantly larger than the predicted value at 2004-DOY-212T05:00:00 (see the top right subplot of Fig. 7). Incomplete drag torque compensation happened because of the “spiky” nature of the drag torque as well as the truncation of the estimated drag torque by the “Drag Torque Limiter” (DTL, see Fig. 2) in the flight software. The DTL was used to remove any unreasonably large drag estimate generated by the estimator. The threshold of the DTL was set at 30 mNm. It was thought that drag torque, even when the RWA is operated at a peak rate of  $\approx 2,000$  rpm, will not exceed this selected threshold. Unfortunately, when the physical drag is indeed very large, the use of DTL will further escalate the difference between the actual and estimated drag torque. Also, due to this truncation, the actual magnitude of the physical drag spike was never known.

As a result of the incomplete drag torque compensation, the RWA-1 controller had difficulty in maintaining the commanded RWA-1 spin rate. RWA rate error  $> 84$  rpm was observed (see top-left subplot of Fig. 8). This level of RWA rate error represented about 42% of the threshold of the monitor entitled “Excessive RWA Rate Control Error” (ERRCE). Similar scenarios were observed on 2004-DOY-227, -260, -271, and -273. On 2004-DOY-273, 64% of the ERRCE’s threshold was exceeded. Had it been triggered, a control mode transition from RWA to RCS thruster would have been commanded by the Safing algorithm.<sup>6</sup> If the safe mode is triggered, all stored sequences onboard will stop executing, and the impacts to the mission is significant. This anomaly had resulted in several corrective actions including an increase in the threshold of DTL as well as the threshold and persistence limit of the ERRCE monitors (of all active RWA). Both the attitude control errors of the S/C’s Y and Z-axis were as large as  $40 \mu\text{rad}$  (see the right subplots of Fig. 8). But these perturbations are not too important in this rolling science observation scenario.

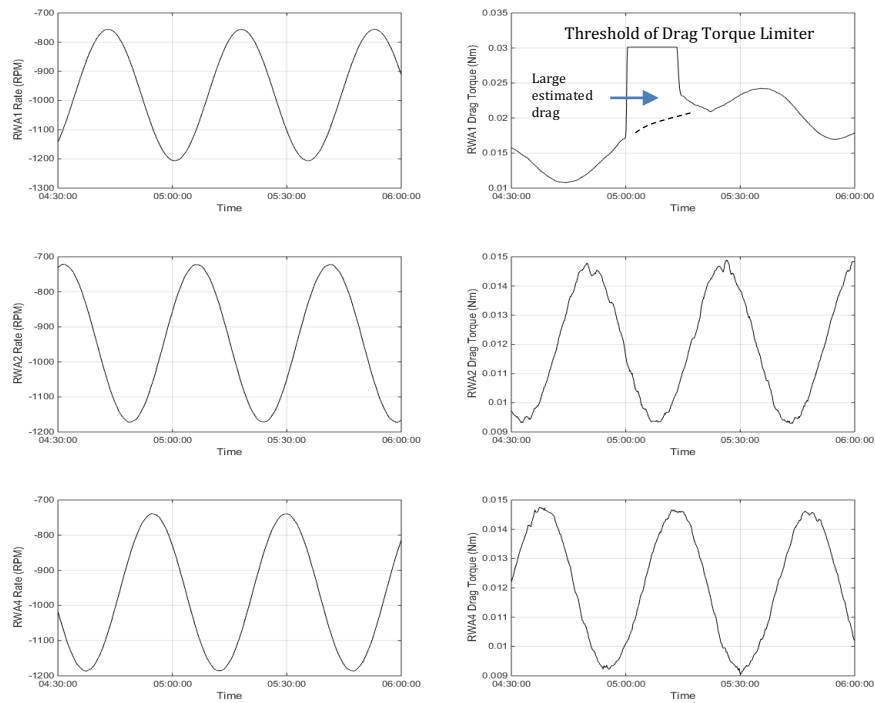


**Fig. 7 A Large RWA-1 Drag Torque Unexpectedly Occurred on 2004-DOY-212.**

## V. Drag Torque Compensation Approaches Studied in Literature

If a system with drag torque is to be operated only at relative high rates without changing spin direction, (i.e., no zero-crossing), drag torque can be adequately modeled as proportional to the spin rate. Under this assumption, classical linear controller design techniques can be used. On the other hand, if the system must operate at low rates with frequent rate reversals, then the linear controller design technique may produce results that are inadequate.

It is well-known that the pointing system performance degradation due to bearing drag torque may be partially compensated with the use of high system gain. But there are disadvantages such as introducing instability into the system as well as saturating the control actuators (as well as the allocated power). Nevertheless, the feasibility of this simple remedy should be investigated before other more elaborate control schemes are explored. As such, in Section V.1 of this paper, we first consider how the current Cassini drag-torque compensator design may be modified using the “high-gain” approach.

Past research works (e.g., Refs. 7–8) had demonstrated the feasibility of reducing the effects of friction/drag (in this paper, the words friction and drag are used interchangeably) on servomechanisms. If a good friction model is not available, an “adaptive observer” is used to estimate friction using measured quantities such as spin rate, etc. (see Section V.2). An example of adaptive friction-compensating system is described in Ref. 9. If a good friction model is available, a model-based friction compensation scheme could be used. In this approach, the friction force  $F$  is estimated using the model, and a signal that compensates for the estimated friction force  $\hat{F}$  is added to control signal (see Section V.3). An example of model-based control technique is given in Ref. 10. Ref. 8 provided a comprehensive comparison between experimental results obtained with different friction-compensating control schemes. It concluded that all these nonlinear controllers can provide better tracking performance when compared to the classical PID-type controller. Results given in Ref. 8, together with those independently reported in Refs. 9–11 provide evidence for the general applicability of these adaptive and model-based friction-compensating control schemes. Ref. 12 gives a comprehensive survey of friction-compensating controller schemes up to the year 1994.

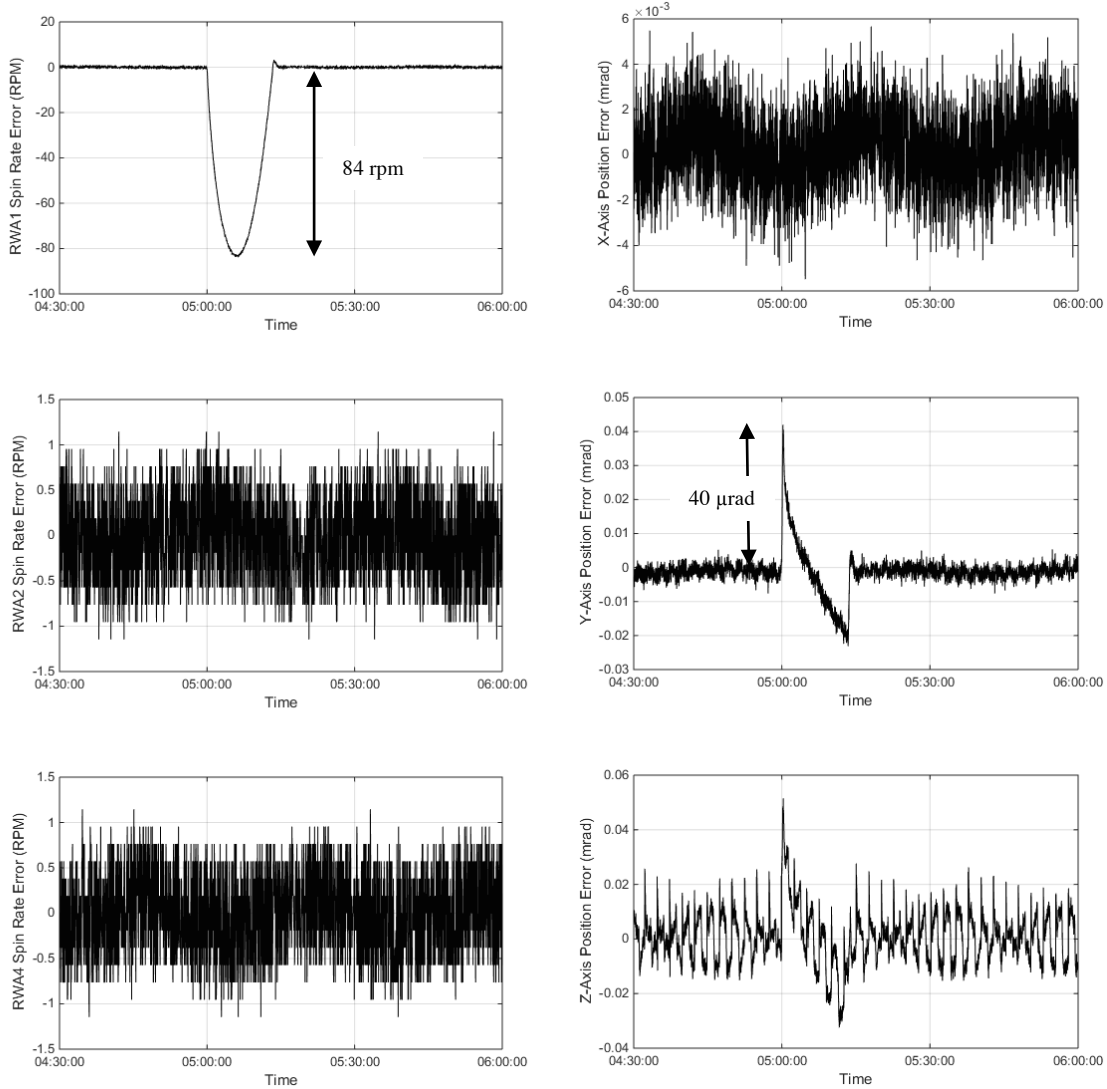


**Fig. 8. A Large RWA Rate Control Error Triggered by An Incomplete Drag Torque Compensation on 2004-DOY-212.**

In early 2000, extended Kalman-Bucy filter (EKBF)-based friction-compensating methods had been introduced. These methods append the friction state to the system state using a Gauss-Markov formulation, and no attempt is made to capture the surface-level friction model in this control scheme. Instead, friction is just calculated using simple Newtonian dynamics based on the well-known plant model and motion measurements. Ref. 13–14 describe these EKBF-based friction-compensating methods. It will be briefly reviewed in Section V.4. Friction compensation via command shaping is briefly reviewed in Section V.5.

Since static and dynamic friction models will be mentioned in the following sections, these friction models are briefly reviewed in the following paragraphs. The static friction model assumes the following expression.

$$F = \text{sgn}(v)[F_C + (F_S - F_C) \exp\left\{-\left(\frac{v}{v_S}\right)^2\right\} + Cv] \quad (3)$$

where  $v$  [m/s] is the relative velocity between the two contacting surfaces,  $F$  is to the total frictional force (N),  $F_C$  is the Coulomb friction (N),  $F_S$  is the stiction friction (N),  $C$  is the viscous friction coefficient (Ns/m),  $v_S$  is the “critical” Stribeck velocity (m/s), the term  $\exp[-(v/v_S)^2]$  models the Stribeck effect (the phenomenon of friction decreasing and then increasing with velocity), and  $\text{sgn}(\bullet)$  is the signum (or sign)

function. Note that, transitioning from  $v = 0+$  to  $0-$  involves a discontinuous change in the friction force (or drag torque).

It is well known that static friction models do not capture many observed friction traits such as hysteresis<sup>#</sup>, frictional lag, and stick-slip motion<sup>∇</sup>. In particular, experiments performed and documented in Ref. 29 show that friction in the vicinity of zero crossing is a dynamic phenomenon that static models failed to adequately describe. Hence, friction models involving dynamics are needed to better describe the physics of frictional phenomenon. A representative dynamic friction model is the Dahl's model introduced in Ref. 15. The LuGre (Lund-Greoble) model is an extension of the Dahl's model.<sup>16,30</sup> Dahl made his initial observation of non-linear friction effects while studying the behavior of ball bearings acted on by low amplitude input forces. At low amplitudes and low frequencies, ball bearings provide some elastic resistance to input forces before they finally are permanently displaced. This elasticity results in hysteresis. At loads below  $F_C$  (Coulomb friction), release of the load allows the balls to return to their initial position. But if a larger load is applied, there will be a permanent displacement after the load is released. One way to describe the Dahl model is as follows:

$$\frac{dz}{dt} = v - \sigma_0 \frac{|v|}{F_C} z, \quad F = \sigma_0 z. \quad (4)$$

In Eq. (4),  $z$  [m] denotes the average bristle (surface asperity) deflection. The interactions between bristles of the two contacting surfaces lead to friction.<sup>12</sup> The parameter  $\sigma_0$  [N/m] is the stiffness (or "spring constant") of the bristles, and  $v$  [m/s] is the relative velocity. The Dahl's model assumes friction force is dependent on displacement only. Others dispute that premise and emphasize the importance of velocity effects, which are especially dominant in the friction behavior of lubricated contact surfaces. The most basic velocity dependencies are the viscous damping and the Stribeck effect given in Eq. (3). The LuGre model modifies the Dahl's model by assuming that friction force varies with not only the bristle deflection  $z$ , but also bristle deflection velocity  $\dot{z}$  and  $v$ . One way to describe the LuGre model is given below.<sup>16,30</sup>

$$g(v) = F_C + (F_S - F_C) \exp \left\{ - \left( \frac{v}{v_S} \right)^2 \right\}$$

$$\frac{dz}{dt} = v - \sigma_0 \frac{|v|}{g(v)} z, \quad F = \sigma_0 z + C_1 \frac{dz}{dt} + C_2 v. \quad (5)$$

In Eq. (5), both  $C_1$  and  $C_2$  have unit of Ns/m (comparable to the viscous coefficient  $C$  in Eq. (3)). Other parameters such as  $F_C$ ,  $F_S$ ,  $v$ ,  $v_S$ , and  $\sigma_0$  were defined in Eqs. (3) and (4). As mentioned in the literature, the challenge in using these dynamics models is in the estimation of the model parameters.

### V.1 Increase the Gain of the Cassini RWA Rate Controller Design.

The gains of the PI drag torque estimator depicted in Fig. 2 are selected to be:  $K_P = 2\xi_D \omega_D I_{RWA}$  and  $K_I = \omega_D^2 I_{RWA}$ . Here,  $\omega_D$  and  $\xi_D$  are the bandwidth and damping ratio of the rate control loop. The bandwidth  $\omega_D$  is selected to be 0.01 Hz (and  $\xi_D$  is 0.707). The resultant gain and phase margins of the RWA rate control loop are 35 dB and  $56^\circ$ , respectively.<sup>2</sup> The selection of a lower bandwidth results in more sluggish wheel response to drag disturbances, which is undesirable. Higher bandwidths than that selected will degrade phase and gain margins. However, the current set of stability margins have healthy margins. Hence, raising the bandwidth  $\omega_D$  could be explored to improve the tracking performance of the RWA drag torque estimator.

In Fig. 3, the peak "delta" magnitude of the physical drag is 2.5 mNm (in 10 s) while the peak estimated drag torque is only 0.6 mNm. The difference is as large as 1.9 mNm. Based on Eq. (1), the derived upper bound on the difference between the physical and estimated drag at time  $T$  is given by  $\Delta(T)$ :

$$\Delta(T) = A \frac{e^{-\omega_D \xi_D T}}{\omega_D \sqrt{1 - \xi_D^2}} \quad (6)$$

<sup>#</sup>The relation between drag torque and velocity measured for increasing velocity is different from that measured for decreasing velocity. This phenomenon is sometime referred to as "hysteresis."

<sup>∇</sup>Stick-slip motion is a common behavior associated with friction. Everyday examples are the squeaking sounds when opening a door or writing on a blackboard with a chalk. In these scenarios, the motion of the object is periodic and alternated between stop ("stick") and motion ("slip"). They could be explained via the LuGre dynamic friction model of Eq. (5).<sup>30</sup>

where “A” is the rate of drag torque change (2.5 mNm/10 s or 0.25 mNm/s). Note that the larger  $\omega_D$  is, the smaller will be  $\Delta$ . With  $\omega_D = 2\pi(0.01)$  rad/s,  $\xi_D = 0.707$ , and  $T = 10$  s, the resultant  $\Delta \approx 3.6$  mNm, which bounded the actual difference of 1.9 mNm. If  $\omega_D$  is doubled,  $\Delta$  will be 1.2 (instead of 3.6) mNm. That is, the estimated drag will better track the physical drag. However, the acceptability of the corresponding drops in gain and phase margins must be ascertained.

## V.2 Adaptive friction compensation schemes<sup>8,9,11-12</sup>

The first application of the adaptive friction compensating system was on a 24-inch telescope located at the Goddard Optical Research Facility.<sup>9</sup> The technique is called a Model Reference Adaptive Control (MRAC) approach. The development of this technique was motivated by the proposed usage in future experiments of lasers having narrow beam widths. The dynamic tracking accuracy requirements were as severe as  $0.78 \mu\text{rad}$  in the presence of varying plant inertia and bearing rate reversals. Details of this model reference adaptive control scheme are given in Ref. 9. A block diagram of MRAC is given in Fig. 9.

Systems for attitude control typically have a cascade structure with a rate control loop and an attitude control loop. Since friction appears in the inner loop, it would be advantageous to introduce friction compensation in that loop. This is indeed the case for the MRAC scheme as depicted in Fig. 9. The reference model depicted near the top of Fig. 9 is a first-order ideal model of the load and tachometer, based on the nominal values of the system parameters. Its output  $v_M$ , the reference rate, is compared with the measured rate  $v$ , and the difference between  $v_M$  and  $v$  ( $e$ ) is used by the adaptive friction observer to update the friction-compensation gains.<sup>9</sup> To be an effective friction compensation system, the bearing rate  $v$  must be measured with good accuracy. One of the key estimates of the adaptive friction observer is  $\hat{F}$ , the estimated friction. It is summed with the control force generated by the linear controller, and is used to negate the physical friction  $F$ .

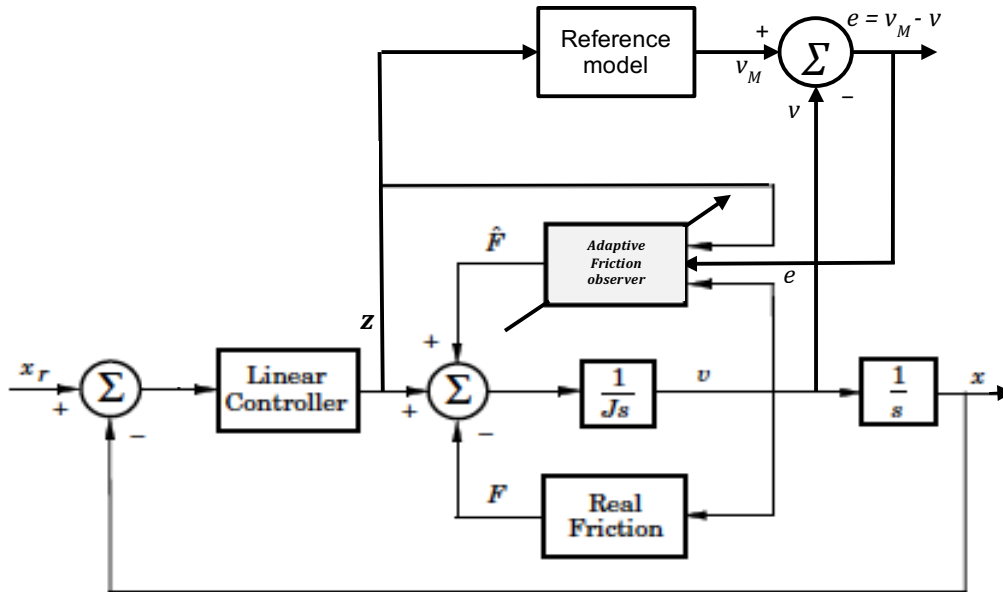


Fig. 9. Block diagram of A Model Reference Adaptive Control Scheme

The global asymptotic stability of the MRAC was proven via the Lyapunov’s direct method. Utilizing the adaptive scheme, the telescope mount would drive at a low rate to within  $0.53 \mu\text{rad}$  peak-to-peak position error. Without the adaptive compensation, a peak-to-peak error of  $6.8 \mu\text{rad}$  would result. This represents a 12:1 improvement. Furthermore, when the velocity command signal passed through the null point, the adaptive compensation virtually eliminated the discontinuity region caused by friction. Refs. 8 and 11 documented other applications of the MRAC scheme. A conclusion given in Ref. 8 is that the sampling rate of the controller play an important role in the performance of these friction compensating systems. For example, when the sampling rate of the MRAC was doubled from 50 to 100 Hz (for the experimental work done in Ref. 8), the researchers observed a significant improvement in the tracking

performance of these nonlinear controllers. This improved performance may be explained by the fact that an instantaneous (discontinuous) change in friction is not as prolonged when the sampling rate is increased.

### V.3 Estimation-based Friction Compensation Schemes<sup>10, 12</sup>

If frictional torque can be accurately predicted in real-time, then a counteracting command can be applied to the system to negate the effect of the frictional torque. With it, the stabilization error will not be proportional to the full frictional torque. Instead, the stabilization error will be proportional to the much smaller mismatch between the actual frictional torque and that predicted by the model. Furthermore, if the predicted frictional torque is adaptively adjusted into agreement with actual friction behavior by processing inputs from other system sensor measurement data (e.g., tachometer), then the results will be robust with respect to changes in bearing drag performance (as mentioned in Section IV). Ref. 10 gives an example.

In Ref. 10, the author studied the stabilization of airborne pointing and tracking telescope. For such a system, the gimbal bearing friction behavior at rate reversals could not be modeled adequately by static friction model. Hence, a dynamic friction model is used instead. To this end, the author postulated the following first-order model for the bearing drag torque  $T_f$ :

$$\tau \frac{dT_f}{dt} + T_f = T_C \operatorname{sgn}(\omega) \quad (7)$$

where  $T_C$  is the bearing Coulomb friction,  $\tau$  is a time constant that is determined experimentally,<sup>8,10</sup> and  $\omega$  is the bearing spin rate. The predicted bearing drag torque  $T_f$  is added to the proportional feedback term to cancel the effect of friction during tracking. The value of  $\tau$  was also updated by this friction-compensating controller since it varies with the operating condition (see Ref. 10 for details). The performance of this friction-compensating scheme had been verified experimentally. The author of Ref. 10 reported a 5:1 improvement in the root-mean-square tracking error (relative to that obtained with the classical PID approach). The stability of this control scheme wasn't proven in Ref. 10, but the stability for a similar friction-compensating control scheme had been established in Ref. 8. However, the authors of both Ref. 8 and Ref. 10 pointed out the difficulty in tuning the free parameters of the dynamic friction model (e.g., the time constant  $\tau$  and the Coulomb friction  $T_C$ ).

### V.4 EKBF-based Friction-compensating Methods<sup>13-14</sup>

The EKBF-based friction-compensating method is a non-model-based friction-compensating control scheme. In this control scheme, a friction estimator is constructed by treating the friction torque as an unknown state element. As depicted in Fig. 10 (from Ref. 14), by measuring motion along with applied force (or torque) and knowing the system parameters (usually, parameters such as inertia properties of the “plant” are known accurately), one can estimate the unknown friction torque required to produce the observed motion. The estimated friction is then used to compensate for the physical drag torque of the position (or attitude) control system. Based on both simulation and experimental results, the authors of Refs. 13–14 conclude that EKBF-based friction estimates compared well to those estimated via model-based friction estimation schemes reviewed in Sections V.2 and V.3. However, they note that EKBF-based methods work on the assumptions that the plant dynamics (e.g., the inertia properties of the “plant”) are known accurately. If this is not the case, model-based compensation schemes (e.g., Refs. 8–12) may be more useful.

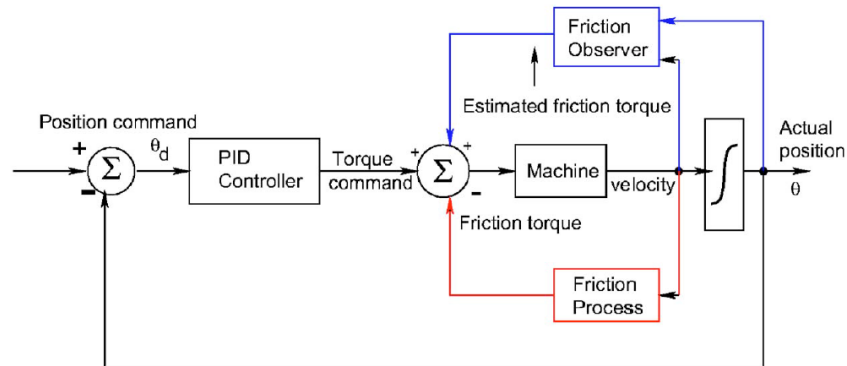


Fig. 10. A Position Control System with A Friction Compensator (see Fig. 1 of Ref. 14)

### **V.5 Friction Compensation Via Command Shaping<sup>17-18</sup>**

The friction discontinuity at a RWA rate reversal causes an undesirable impulsive jerk disturbance to the spacecraft. As a consequence, the pointing stability performance of the spacecraft might degrade. In order to deal with this disturbance, the authors of Ref. 17 proposed a “command shaping” technique. To this end, the bearing drag torque is modeled using an expression similar to Eq. (3), with a drag torque discontinuity at zero velocity. In Ref. 17, the discontinuous drag torque is shaped using a parabolic function in order to “smooth” out the abrupt change of frictional torque when the reaction wheel crosses the zero speed. The three shaping parameters of the parabolic function are selected to meet a set of boundary conditions. Closed-form expressions of these parameters are given in Ref. 17, making them suitable for implementation in flight software. In this “command shaping” approach, the control torque generated by the linear PID controller is augmented with a “shaped” friction compensation torque. The proposed method is evaluated using a nonlinear simulation of an attitude control system composed of a quaternion-based PID controller, four reaction wheels with nonlinear friction model, spacecraft dynamics, kinematics, etc. The effectiveness of the proposed command shaping to deal with the nonlinearity of the reaction wheel is confirmed via these simulation works. See also results from Ref. 18.

### **V.6 Dither-based Friction Compensation Methods<sup>12, 19-20</sup>**

Traditionally, control engineers have used open-loop “smoothing” techniques such as dither to deal with the discontinuous drag torque that happened during bearing rate reversals.<sup>12</sup> The dither-introduced oscillation will keep the system in motion continuously, avoiding the stiction friction. Hence, dither signal, with alternating polarity, can average out the system discontinuity dynamics, and a nearly continuous and “linear” system is produced. Classical control techniques can then be applied on this “linear” system. The author of Ref. 19 had proven analytically that with dither, abrupt static friction disturbances could be eliminated and near linear behavior through zero rate is achieved. However, the addition of a dither signal to the reaction wheel control torque can also excite selected spacecraft structural modes, lead to significant chattering phenomenon in the spacecraft body rate. This will threaten selected spacecraft pointing stability requirements.

### **V.7 Other Friction Compensation Methods<sup>21-26</sup>**

There are numerous other friction-compensating control schemes given in the literatures. In Ref. 21, a sliding mode controller with a friction observer is used to perform attitude maneuvers in the presence of low-speed bearing friction and other external disturbances. Simulation results indicate that the proposed friction-compensating controller has better transient and steady-state performance relative to that designed using classical linear control techniques. In Ref. 22, a friction compensator was designed based on the LuGre friction model (see Eq. (5)) that captured Coulomb friction, viscous friction, stiction friction, and the Stribeck effects. Simulation results were shown for a set of spacecraft maneuvers indicating significant improvement in the attitude and rate tracking error. Performance of other friction-compensating control schemes are described in Refs. 23–27.

## **VI. Summary**

A high level of spacecraft-pointing stability is needed during imaging operations of most optical remote sensing instruments.<sup>31</sup> Typically, the required level of pointing stability is only achievable using a set of reaction wheels. As illustrated by multiple sets of Cassini flight data, RWA spin rate reversals will degrade the pointing stability performance of the attitude control system. The RWA bearing drag performance of both the NASA Cassini and ESA XMM-Newton missions were documented in Ref. 4. The RWA bearings of these spacecraft had experienced anomalous and “spiky” drag torques at unpredictable times. Unless the drag torque compensation system of the RWA controller could deal with these abrupt drag changes, the S/C pointing stability performance would also degrade. For Cassini, this wasn’t a problem because of the significant performance margin in pointing stability. However, for missions with very challenging pointing stability requirements, the implementation of an effective drag-compensating control schemes will be critical. Since the early 60’s, many friction-compensating control schemes such as the model-reference adaptive control have been studied. A limited-scope literature survey of these friction compensations schemes is given in this paper. Many of these nonlinear control schemes can achieve good pointing control performance even with repetitive RWA rate reversals. The feasibility of incorporating selected design features used in these proven friction-compensation schemes should be explored. The

estimated drag torque, either nominal or anomalous, could also be made available to the mission operations team. Via trending, ground operators can monitor the long-term health of the reaction wheels.

### Acknowledgements

The work described in this paper was carried out by Jet Propulsion Laboratory, California Institute of Technology, under a contract with the National Aeronautics and Space Administration. I wish to thank Luis G. Andrade, a member of the Cassini mission operation team, for invaluable supports. I also want to thank Todd S. Brown and Joan Stupik for their valuable reviews of an earlier version of this paper. The encouragement and support of Julie L. Webster is also acknowledged.

### References

- <sup>1</sup>Lee, A.Y. and Hanover, G., "Cassini Spacecraft Attitude Control Flight Performance," AIAA-2005-6269, Proceedings of the AIAA Guidance, Navigation, and Control Conference, San Francisco, California, 15–18 August 2005.
- <sup>2</sup>Macala, G. A., "Design of the Reaction Wheel Attitude Control System for the Cassini Spacecraft," AAS Paper 02-121, pp. 27–30, January 2002.
- <sup>3</sup>Pilinski, E. and Lee, A.Y., "Pointing Stability Performance of the Cassini Spacecraft," *Journal of Spacecraft and Rockets*, Volume 46, No. 5, September-October, 2009, pp. 1007–1015.
- <sup>4</sup>Lee, A.Y. and Wang, E.K., "Inflight Performance of Cassini Reaction Wheel Bearing Drag in 1997–2013," *Journal of Spacecraft and Rockets*, Vol. 52, No. 2, March–April, 2015, pp. 470–480.
- <sup>5</sup>Ekinci, M.F., "Solar Dynamics Observatory Reaction Wheel Bearing Friction Increase: Detection, Analysis, and Impacts," 13<sup>th</sup> International Conference on Space Operations, SpaceOps 2014, May 5–9, 2014.
- <sup>6</sup>Lee, A.Y. and Burk, T.A., "Cassini Spacecraft Attitude Control System Flight Performance and Lessons Learned, 1997–2017," AIAA SciTech, Kissimmee, Florida, AIAA Guidance, Navigation, and Control Conference, 8–12 January 2018.
- <sup>7</sup>Olsson H., Åström, K.J., Canudas de Wit, C., Gafvert, M., and Lischinsky, P., "Friction Models and Friction Compensation," *European Journal of Control*, Vol. 4, Issue 3, pp. 176–195, 1998.
- <sup>8</sup>Leonard, N.E. and Krishnaprasad, P.S., "Adaptive Friction Compensation for Bi-directional Low-velocity Position Tracking," 31<sup>st</sup> IEEE Conference on Decision and Control, December 1992, pp. 267–273.
- <sup>9</sup>Gilbart, J. and Winston, G., "Adaptive Compensation for an Optical Tracking Telescope," *Automatica*, 10:125–131, 1974.
- <sup>10</sup>Walrath, C.D., "Adaptive Bearing Friction Compensation Based on Recent Knowledge of Dynamic Friction," *Automatica*, 20(6):717–727, 1984.
- <sup>11</sup>Canudas deWit, C., Åström, K.J., and K. Braun, "Adaptive Friction Compensation in DC Motor Drives," *IEEE Journal of Robotics and Automation*, RA-3(6):681–685, 1987.
- <sup>12</sup>Armstrong-Hélouvry, B., Dupont, P., and Canudas de Wit, C., "A Survey of Models, Analysis Tools and Compensation Methods for the Control of Machines with Friction," *Automatica*, 30, pp. 1083–1138, 1994.
- <sup>13</sup>Ray, L.R., Ramasubramanian, A. and Townsend, J.R., "Adaptive Friction Compensation Using Extended Kalman Bucy Filter Friction Estimation," *Control Engineering Practices*, 9, 2001, pp. 169–179.
- <sup>14</sup>Ramasubramanian, A. and Ray, L.R., "Comparison of EKBF-based and Classical Friction Compensation," *Transaction of the ASME*, Vol. 129, March 2007.
- <sup>15</sup>Dahl, P., "Measurement of Solid Friction Parameters of Ball Bearings," Proceedings of the Sixth Annual Symposium on Incremental Motion Control and Devices (pp. 49–60), University of Illinois, Urbana, IL, USA, 1977.
- <sup>16</sup>Canudas deWit, C., Olsson, H., Åström, K. J., and Lischinsky, P., "A New Model for Control of Systems with Friction," 40(3), 1995.
- <sup>17</sup>Lee, S.H., Kim, J.H., Lee, S.R., "Low-speed Friction Compensation of Reaction Wheels Using Command Shaping," Proceedings of the IEEE International Conference on Industrial Technology, pp. 106–111, February 25–28, 2013.
- <sup>18</sup>Hekman, K., Lawrence, J., and Singhose, W. "Use of Input Shaping to Decrease the Effects of Stiction," in 5<sup>th</sup> IFAC Symposium on Nonlinear Control Systems, St. Petersburg, Russia, 2001.
- <sup>19</sup>Stetson, J.B., Jr., "Reaction Wheel Low-speed Compensation Using a Dither Signal," *Journal of Guidance, Control, and Dynamics*, Vol. 16, No. 4, pp. 617–622, Jul-Aug 1993.

- <sup>20</sup>Stetson, J.B., Jr., “Reaction Wheel Friction Compensation Using Dither,” US Patent #5,020,745, 1991.
- <sup>21</sup>Wu, S., Wang, R., Radice, G., and Wu, Z., “Robust Attitude Maneuver Control of Spacecraft with Reaction Wheel Low-speed Friction Compensation,” *Aerospace Science and Technology*, Vol. 43, pp. 213–218, June 2015.
- <sup>22</sup>Hill, D.E., “Dynamics and Control of Spacecraft Using Control Moment Gyros with Friction Compensation,” *Journal of Guidance, Control, and Dynamics*, Vol. 39, No. 10, pp. 2405–2417, 2016.
- <sup>23</sup>Chiu, M.C. and Liaw, C.M., “Dynamic Control and Diagnostic Friction Estimation for an SPMSM-Driven Satellite Reaction Wheel,” *IEEE Transactions on Industrial Electronics*, Vol. 58, No. 10, October 2011, pp. 4693–4707.
- <sup>24</sup>Stajic, D., Peric, N., and Deur, J., “Friction Compensation Methods in Position and Speed Control Systems” *Proceedings of the IEEE International Symposium on Industrial Electronics*, February 1999.
- <sup>25</sup>Bauer, R.J., Hong, T., and Hughes, P.C., “Augmented System Identification of Reaction Wheel Friction,” *Canadian Aeronautics and Space Journal*, Vol. 47, No. 2, pp. 51–55, June 2001.
- <sup>26</sup>Carrara, V. and Kuga, H.K., “Estimating Friction Parameters in Reaction Wheels for Attitude Control,” *Mathematical Problems in Engineering*, 2013, Article ID 249674.
- <sup>27</sup>Amin, J., Friedland, B., and Harnoy, A., “Implementation of a Friction Estimation and compensation Technique,” *IEEE Control Systems*, August 1997, pp. 71–76.
- <sup>28</sup>Harnoy, A., Friedland, B., and Cohn, S., “Modeling and Measuring Friction Effects,” *IEEE Control Systems Magazine*, Vol. 28, No. 6, pp. 82–91, December 2008.
- <sup>29</sup>Haessig, D.A., Jr., and Friedland, B., “On the Modeling and Simulation of Friction,” *Trans. ASME, Journal of Dynamic Systems, Measurement, and Control*, Vol. 113, pp. 354–361, September 1991.
- <sup>30</sup>Åström, K. J. and Canudas de Wit, C., “Revisiting the LuGre Friction Model,” *IEEE Control Systems*, Vol. 28, No. 6, pp. 101–114, 2008.
- <sup>31</sup>Blackmore, L., Murray, E., Scharf, D.P., Aung, M., Bayard, D., Brugarolas, P., Hadaegh, F., Kang, B., Lee, A.Y., Milman, M., and Sirlin, S., “Instrument Pointing Capabilities: Past, Present, and Future,” Paper AAS 11-091, 34<sup>th</sup> AAS Annual Rocky Mountain Guidance and Control Conference, Breckenridge, Colorado, February 4–9, 2011.

### Acronyms

<i>AACS</i>	= Attitude and Articulation Control Subsystem
<i>CIRS</i>	= Composite Infrared Spectrometer
<i>CW</i>	= Clockwise
<i>CCW</i>	= Counter-Clockwise
<i>DOY</i>	= Day of the Year
<i>DTL</i>	= Drag Torque Limiter
<i>EHD</i>	= Elasto-Hydro-Dynamic
<i>EKBF</i>	= Extended Kalman-Bucy Filter
<i>ERRCE</i>	= Excessive RWA Rate Control Error (an error monitor)
<i>IRU</i>	= Inertial Reference Unit
LuGre	= Lund-Greoble (Dynamic) Friction Model
<i>MRAC</i>	= Model Reference Adaptive Control
<i>PD</i>	= Proportional and Derivative
<i>RWA</i>	= Reaction Wheel Assembly
<i>RWAC</i>	= Reaction Wheel Attitude Control System
<i>S/C</i>	= Spacecraft
<i>SDO</i>	= Solar Dynamics Observatory
<i>XMM</i>	= X-ray Multi-mirror Mission

**Appendix A**  
**Zero-crossing of Reaction Wheel Rate During a Nadir-pointed Planetary Flyby**

The total angular momentum vector of the spacecraft, as expressed in the spacecraft body frame, has two components:  $H_{\text{Total}} = H_{\text{SC}} + H_{\text{RWA}}$ . The component caused by the spacecraft rates is  $H_{\text{SC}} = I_{\text{SC}}\Omega$ , where  $I_{\text{SC}} = \text{diag}([I_{xx}, I_{yy}, I_{zz}]^T)$ , and  $\Omega = [\omega_x, \omega_y, \omega_z]^T$ . The MOI's of the S/C about the X, Y, and Z-axis are (in the year 2013) [6,400, 5,300, 3,500] kg-m<sup>2</sup>, respectively. To determine the angular momentum of the RWAs, we first define the RWA spin rate vector  $\Delta = [\omega_1, \omega_2, \omega_4]^T$ . Note that the prime RWAs of Cassini are RWA-1, 2, and 4. The coordinate transformation matrix between these RWA and the S/C's XYZ axes, P, is given in Eq. (A1). In this equation,  $e_i$  ( $i = X-Z$ , or 1,2,4) represents a unit vector in the direction of the S/C's  $i$ -axis. To find  $H_{\text{RWA}}$  in the S/C's body coordinates, simply multiply  $\Delta$  by the inertia matrix for the RWAs ( $I_{\text{RWA}}$ , all RWAs have nearly identical inertia, 0.16 kg-m<sup>2</sup>), and then multiply the result by the transformation matrix P.

$$\begin{bmatrix} e_x \\ e_y \\ e_z \end{bmatrix} = [P] \begin{bmatrix} e_1 \\ e_2 \\ e_4 \end{bmatrix} = \begin{bmatrix} 0 & -\frac{1}{\sqrt{2}} & \frac{1}{\sqrt{2}} \\ \frac{\sqrt{2}}{3} & -\frac{1}{\sqrt{6}} & -\frac{1}{\sqrt{6}} \\ \frac{1}{\sqrt{3}} & \frac{1}{\sqrt{3}} & \frac{1}{\sqrt{3}} \end{bmatrix} \begin{bmatrix} e_1 \\ e_2 \\ e_4 \end{bmatrix} \quad (\text{A1})$$

The conservation of total angular momentum of the spacecraft (in the absence of external environmental torque) is only valid in an inertial coordinate system. As such, a transformation matrix Q(t), from the S/C's frame to the J2000 inertial frame, must be defined. To this end, it is convenient to use the S/C's coordinate frame at time  $t = 0$  as the inertial frame (see Fig. A1). With reference to Fig. A1, the transformation matrix Q(t) is given by Eq. (A2). The angle used in Eq. (A2),  $\beta = \alpha - \alpha_0$ , is defined in Fig. A1.

$$Q(t) = \begin{bmatrix} \cos\beta(t) & 0 & +\sin\beta(t) \\ 0 & 1 & 0 \\ -\sin\beta(t) & 0 & \cos\beta(t) \end{bmatrix} \quad (\text{A2})$$

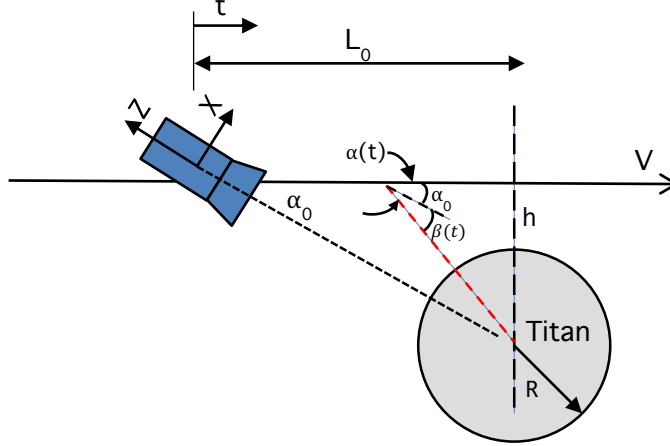


**Fig. A1. A Representative Cassini Flyby of Titan: HGA nadir-pointed at Titan**

In Fig. A1,  $h$  is the flyby altitude at closest approach (1,500 km),  $R$  is the radius of Titan (2,575 km),  $V$  is the constant flyby velocity (6.5 km/s),  $L_0$ ,  $\sqrt{3}(h+R)$  km, is the horizontal distance at the start of the flyby (accordingly,  $\alpha_0$  is 30°). Via simple kinematical relations, the time rate of change of the angle  $\alpha(t)$  is given by Eq. (A3):

$$\frac{d\alpha}{dt} = \frac{V}{h+R} \sin^2\alpha(t) \quad (\text{A3})$$

It is assumed that the selected flyby altitude is such that the Titan atmospheric torque imparted on the S/C is insignificant. As such, the total angular momentum vector is approximately conserved in an inertial frame during a RWA-based target motion compensation slew. Hence, we can estimate the RWAs' spin rate at time  $t$  using the following expression (Eq. (A4)):

$$\begin{bmatrix} \omega_1(t) \\ \omega_2(t) \\ \omega_4(t) \end{bmatrix} \approx P^{-1} I_{RWA}^{-1} I_{YY} \left\{ Q^{-1}(t) \begin{bmatrix} 0 \\ \omega_{y0} \\ 0 \end{bmatrix} - \begin{bmatrix} 0 \\ \omega_y(t) \\ 0 \end{bmatrix} \right\} - P^{-1} Q^{-1}(t) P \begin{bmatrix} \omega_{10} \\ \omega_{20} \\ \omega_{40} \end{bmatrix} \quad (A4)$$

In Eq. (A4),  $[\omega_{10}, \omega_{20}, \omega_{40}]^T$  is the RWAs' spin rate vector, in rad/s, at time  $t = 0$ .  $\omega_y(t)$  is the S/C's Y-axis rate,  $\dot{\alpha}$ , given in Eq. (A3), and  $\omega_{y0}$  is the S/C's Y-axis rate at time  $t = 0$ . Note also that  $Q^{-1}(t) = Q^T(t)$  since  $Q(t)$  is a symmetrical matrix. Using Eqs. (A1), (A2), and (A3), Eq. (A4) is equivalent to the following:

$$\begin{bmatrix} \omega_1(t) \\ \omega_2(t) \\ \omega_4(t) \end{bmatrix} \approx \frac{I_{YY}[\omega_{y0} - \omega_y(t)]}{I_{RWA}} \begin{bmatrix} \sqrt{\frac{2}{3}} \\ -\frac{1}{\sqrt{6}} \\ -\frac{1}{\sqrt{6}} \end{bmatrix} + \begin{bmatrix} \frac{2+\cos\beta}{3} & -\frac{\sin\beta}{\sqrt{6}} + \frac{\cos\beta-1}{3} & \frac{\sin\beta}{\sqrt{6}} + \frac{\cos\beta-1}{3} \\ \frac{\sin\beta}{\sqrt{6}} + \frac{\cos\beta-1}{3} & \frac{1+5\cos\beta}{6} & \frac{2\sin\beta}{\sqrt{6}} + \frac{1-\cos\beta}{6} \\ -\frac{\sin\beta}{\sqrt{6}} + \frac{\cos\beta-1}{3} & -\frac{2\sin\beta}{\sqrt{6}} + \frac{1-\cos\beta}{6} & \frac{1+5\cos\beta}{6} \end{bmatrix} \begin{bmatrix} \omega_{10} \\ \omega_{20} \\ \omega_{40} \end{bmatrix} \quad (A5)$$

The time histories of the RWA spin rates, for eight sets of initial RWA spin rates (see Table A1) are computed using Eq. (A5). The results indicate that, in all cases, at least one of the three RWA spin rates will have “zero-crossing” in the time window of  $T_{\text{closest}} \pm 1086$  s.<sup>#</sup> The approximate times at which the zero-crossing occurred are given in Table A1. Define  $C_1 = +\frac{\omega_{10}}{2} - \left(\frac{1}{2} + \frac{1}{\sqrt{8}}\right)\omega_{20} - \left(\frac{1}{2} - \frac{1}{\sqrt{8}}\right)\omega_{40}$  as the crossing criterion of the time history of  $\omega_1(t)$ . If  $\omega_{10}$  is positive, then the condition “ $C_1 < 0$ ” predicts a zero crossing in the time history of  $\omega_1(t)$ . If  $\omega_{10}$  is negative, then the condition “ $C_1 > 0$ ” predicts a zero crossing in the time history of  $\omega_1(t)$ . Otherwise, there is no zero-crossing. These predictions are confirmed by data given in Table A1. The zero-crossing criteria for  $\omega_2(t)$  and  $\omega_4(t)$  are:  $C_2 = \left(-\frac{1}{2} + \frac{1}{\sqrt{8}}\right)\omega_{10} - \frac{1}{4}\omega_{20} + \left(\frac{1}{4} + \frac{1}{\sqrt{2}}\right)\omega_{40}$ , and  $C_4 = -\left(\frac{1}{2} + \frac{1}{\sqrt{8}}\right)\omega_{10} + \left(\frac{1}{4} - \frac{1}{\sqrt{2}}\right)\omega_{20} - \frac{1}{4}\omega_{40}$ , respectively. Fig. A1 depicts the time histories of the RWA spin rates for four sets of initial RWA spin rates. Time histories of RWA spin rates for other sets of initial RWA spin rates are omitted for brevity.

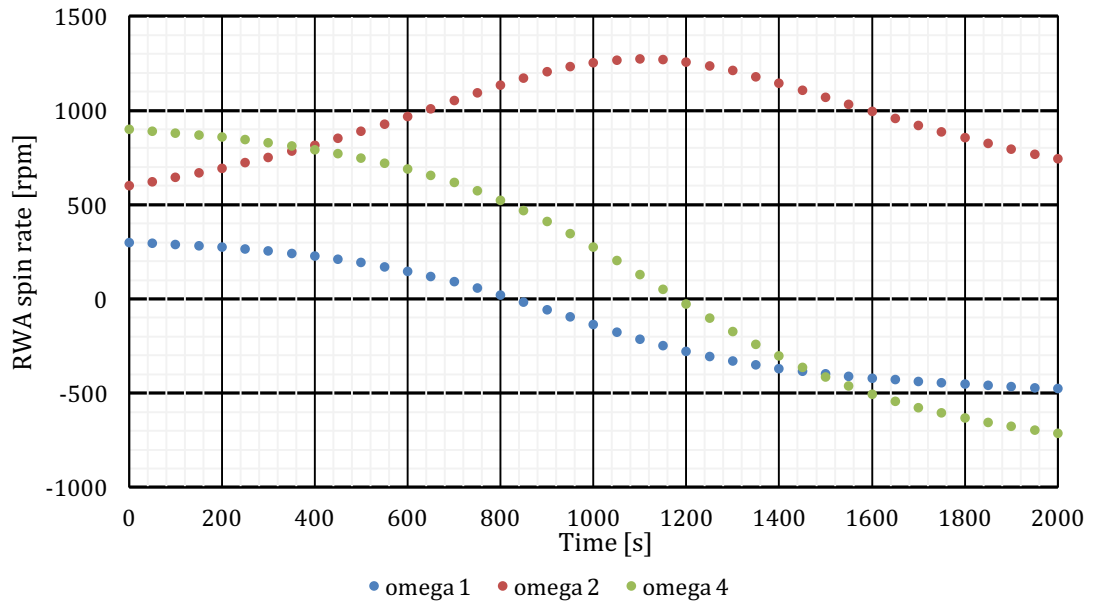
**Table A1. RWA Spin Rate Reversals During a Titan Flyby**

Initial RWAs' Spin rate [rpm]†	Approximate Time at which RWA-1/2/4 Zero-crossing occurred* [s]		
	RWA-1	RWA-2	RWA-4
[300, 600, 900]	800	No crossing	1,200
[300, 600, -900]	500	1,000	No crossing
[300, -600, 900]	No crossing	750	1,800
[300, -600, -900]	No crossing	No crossing	1,250
[-300, 600, -900]	No crossing	900	1,700
[-300, 600, 900]	No crossing	No crossing	1,560
[-300, -600, -900]	1,500	No crossing	1,000
[-300, -600, 900]	1,200	780	No crossing

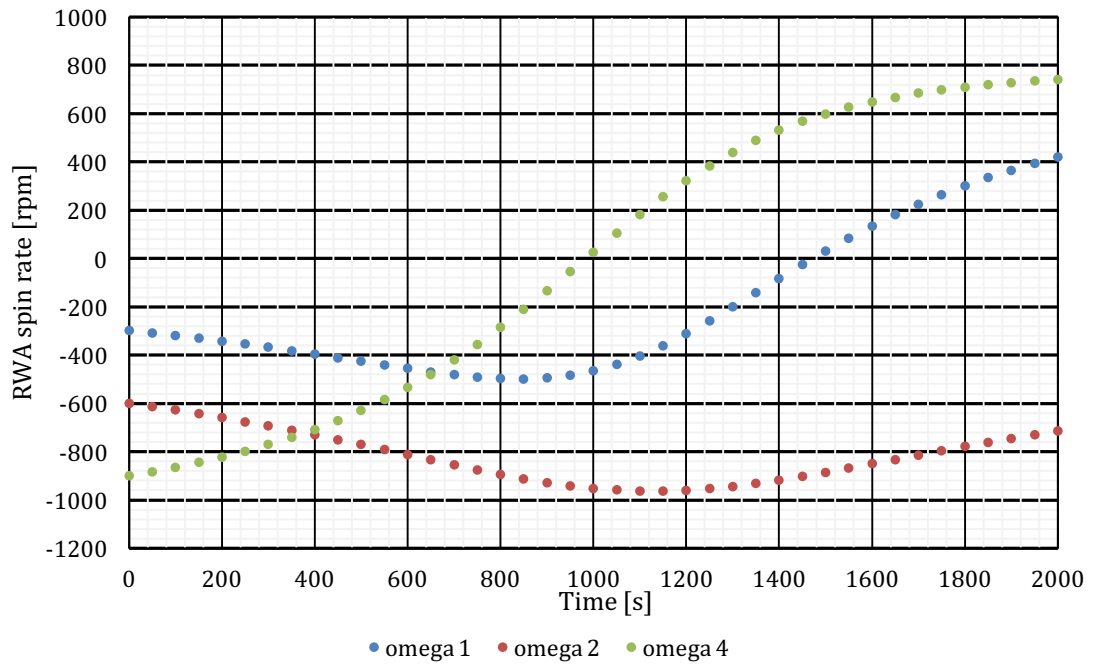
†These set of spin rates were selected arbitrarily. \*The time of Titan closest approach is  $t \approx 1,086$  sec.

<sup>#</sup>The only case without any RWA spin rate zero-crossing is when  $[\omega_{10}, \omega_{20}, \omega_{40}] = [0, 0, 0]$  rpm. However, operating the wheels at near-zero rpm will lead to excessive metal-to-metal contacts between bearing balls and races, and is highly undesirable. See Section III.

[300, 600, 900] rpm



[-300, -600, -900] rpm



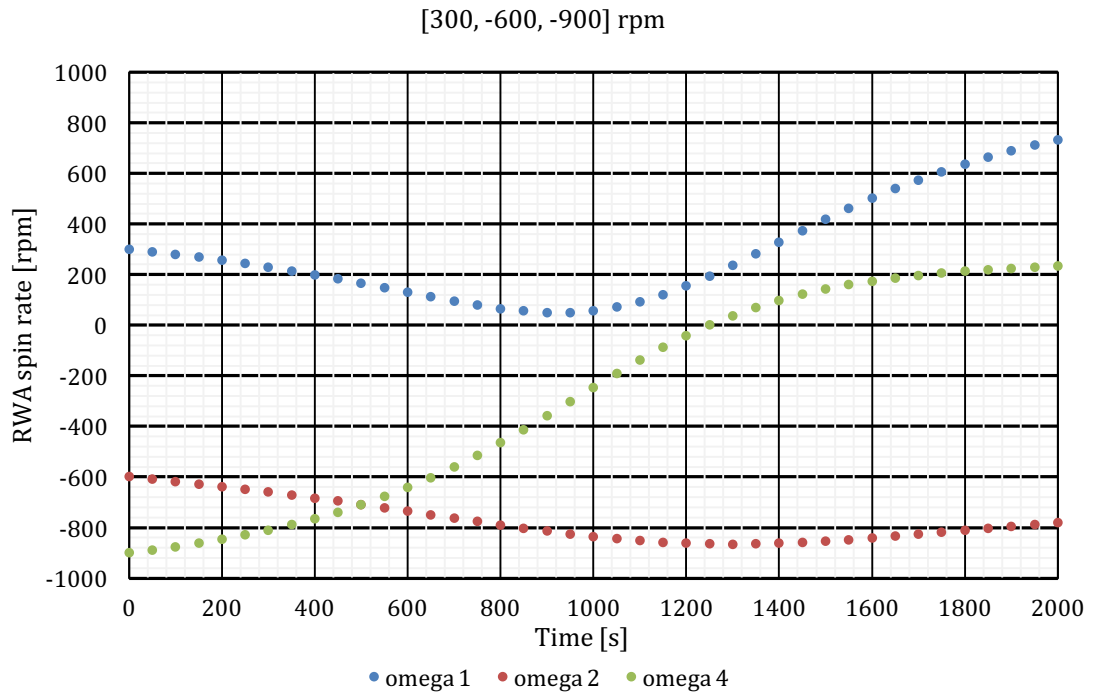
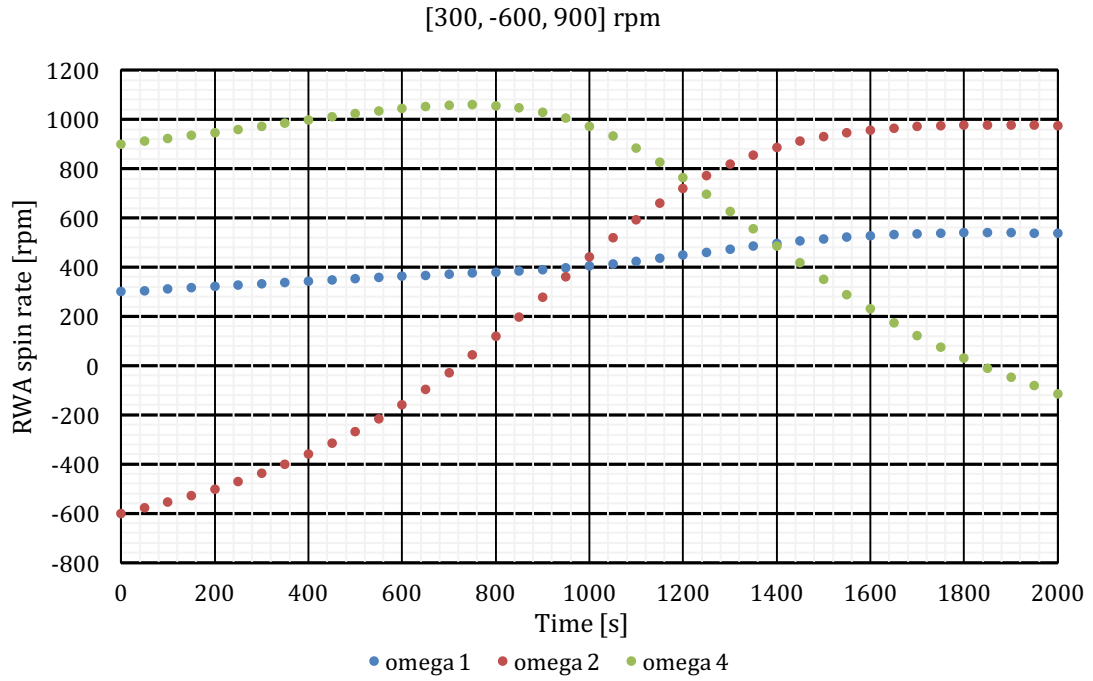


**Fig. A1. Time histories of RWA spin rates during a RWA-based Titan flyby (with four sets of initial RWA spin rates)**

## Appendix B

### Additional Examples of Cassini Attitude Control Transients Triggered by Reaction Wheel Rate Reversals

In Fig. B1, there was a “zero crossing” of the RWA-4 rate near 2013-DOY-005T17:31:12 (as indicated by a bold arrow head) from the CW to the CCW direction. The crossing happened at a rate of -1.8 rpm per second. As a result of the incomplete RWA-4 drag torque compensation, noticeable perturbations in the X and Z-axis S/C’s attitude control errors were observed soon after the crossing. The perturbed rate changes about the X and Z-axis are +1.13 and +1.38  $\mu\text{rad/s}$ , respectively. The corresponding torque impulse estimates are +10.2 and +8.36 milli-Nms (with a mean value of +9.28 milli-Nms). The crossing-induced perturbed rate change about the Y-axis is intertwined with rate changes caused by other Y-axis control activities (see right-center subplot of Fig. B1). No estimation of the zero-crossing torque impulse is attempted using the perturbed Y-axis rate change.

In Fig. B2, there was a “zero crossing” of the RWA-2 rate near 2007-DOY-029T21:10:00 (as indicated by a bold arrow head) from the CW to CCW direction. There was another “zero crossing” of the RWA-1 rate near 2007-DOY-029T21:03:00 (also indicated by a bold arrow head) also from the CW to the CCW direction. Near the time of these two zero-crossings, we see two perturbations in the X-axis attitude control error (top right subplot) and another two Z-axis attitude control error (bottom right subplot). These perturbations are all indicated by dashed arrows. The time history of the Y-axis attitude control error is given in the center right subplot. In this subplot, we also see two large attitude control errors but they are unrelated to the zero crossings. Instead, they occurred as a result of a commanded Y-axis slew. These slew-induced perturbations are an order of magnitude larger than those caused by RWA zero-crossings. As such, those smaller crossing-related perturbations about the Y-axis are harder to observe. To estimate the torque impulse due to the RWA-2 zero crossing, we note the fact the MOI’s of the S/C in early 2007 were [6,882, 5,688, 3,620]  $\text{kg}\cdot\text{m}^2$ . The angles between the spin axis of RWA2 and the S/C’s X, Y, and Z-axis are [135°, 114°, 54.74°], respectively. Accordingly, the estimated magnitudes of the RWA-2 zero crossing-related torque impulse are +12.3 and +11.6 milli-Nms, respectively. The mean magnitude of the torque impulse is 11.9 milli-Nms.

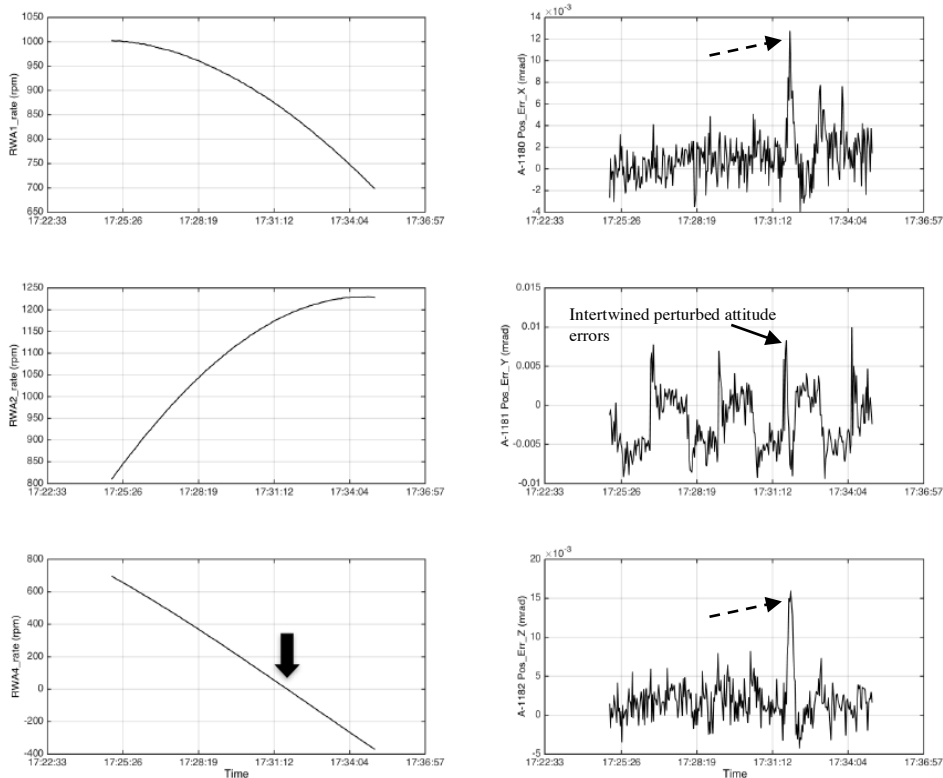


**Fig. B1. Transients of S/C Attitude Control Errors Caused by RWA-4 Rate Reversal**

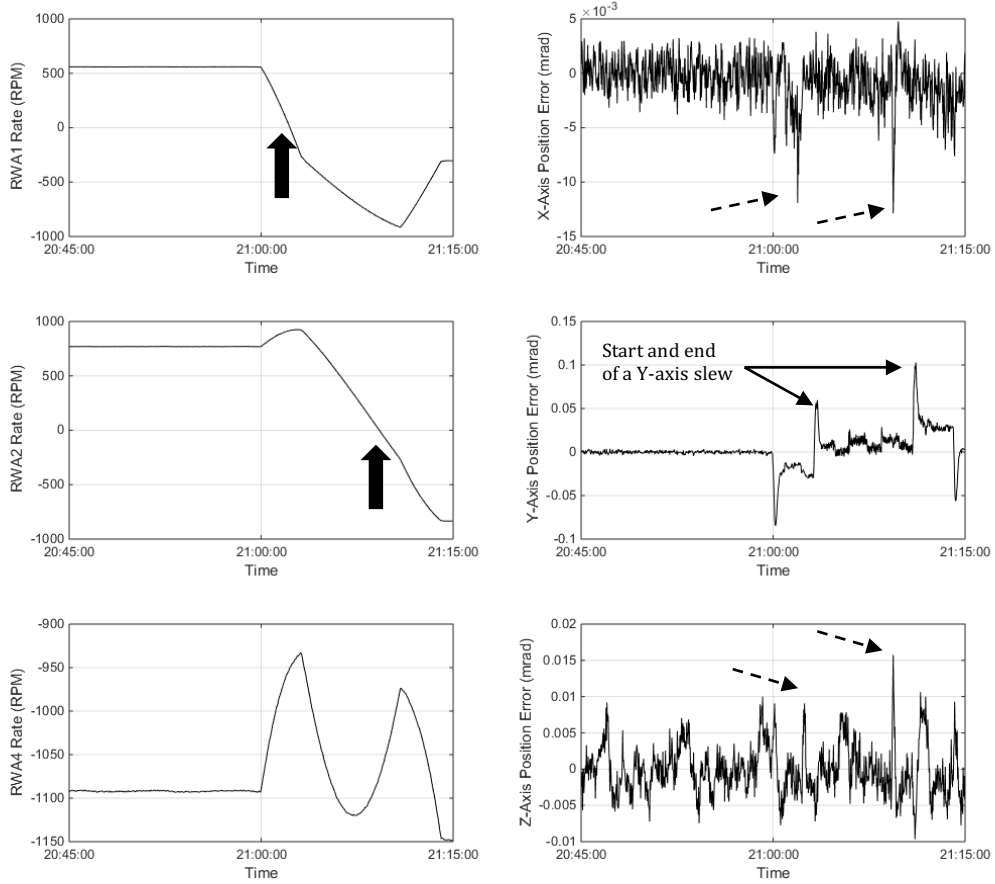


**Fig. B2. Transients of S/C Attitude Control Errors Caused by Two RWA Rate Reversals**